



HHS Public Access

Author manuscript

Oncogene. Author manuscript; available in PMC 2021 October 30.

Published in final edited form as:

Oncogene. 2021 May ; 40(20): 3593–3609. doi:10.1038/s41388-021-01804-7.

Multiple interactions of the oncoprotein transcription factor MYC with the SWI/SNF chromatin remodeler

Chase M. Woodley¹, Alexander S. Romer², Jing Wang^{3,4}, Alissa D. Guarnaccia¹, David L. Elion¹, Jack N. Maxwell², Kiana Guerrazzi¹, Tyler S. McCann¹, Tessa M. Popay¹, Brittany K. Matlock⁵, David K. Flaherty⁵, Shelly L. Lorey¹, Qi Liu^{3,4}, William P. Tansey^{1,6}, April M. Weissmiller^{2,*}

¹Department of Cell and Developmental Biology, Vanderbilt University School of Medicine, Nashville, TN 37240, USA

²Department of Biology, Middle Tennessee State University, Murfreesboro, TN 32132, USA

³Center for Quantitative Sciences, Vanderbilt University Medical Center, Nashville, TN 37240, USA

⁴Department of Biostatistics, Vanderbilt University Medical Center, Nashville, TN 37240, USA

⁵Vanderbilt University Medical Center Flow Cytometry Shared Resource, Vanderbilt University Medical Center, Nashville, TN 37240, USA

⁶Department of Biochemistry, Vanderbilt University School of Medicine, Nashville, TN 37240, USA

Abstract

The SNF5 subunit of the SWI/SNF chromatin remodeling complex has been shown to act as a tumor suppressor through multiple mechanisms, including impairing the ability of the oncoprotein transcription factor MYC to bind chromatin. Beyond SNF5, however, it is unknown to what extent MYC can access additional SWI/SNF subunits or how these interactions affect the ability of MYC to drive transcription particularly in SNF5-null cancers. Here, we report that MYC interacts with multiple SWI/SNF components independent of SNF5. We show that MYC binds the pan-SWI/SNF subunit BAF155 through the BAF155 SWIRM domain, an interaction that is inhibited by the presence of SNF5. In SNF5-null cells, MYC binds with remaining SWI/SNF components to essential genes, although for a purpose that is distinct from chromatin remodeling. Analysis of MYC–SWI/SNF target genes in SNF5-null cells reveals that they are associated with core biological functions of MYC linked to protein synthesis. These data reveal that MYC can bind SWI/SNF in a SNF5-independent manner and that SNF5 modulates access of MYC to core SWI/SNF complexes. This work provides a framework in which to interrogate the influence of SWI/SNF on MYC function in cancers in which SWI/SNF or MYC are altered.

Users may view, print, copy, and download text and data-mine the content in such documents, for the purposes of academic research, subject always to the full Conditions of use: http://www.nature.com/authors/editorial_policies/license.html#terms

*To whom correspondence should be addressed: Department of Biology, Middle Tennessee State University, Mail Box 60, Murfreesboro, TN 37132. Phone: 615-898-5868. april.weissmiller@mtsu.edu.

Competing interests

The authors declare no competing interests.

Introduction

The MYC family of oncogene transcription factors are overexpressed or deregulated in the majority of malignancies (1). The ability of MYC to regulate gene expression has been linked to its interaction with multiple chromatin regulators that are proposed to play important roles in each aspect of the transcription process (2). One chromatin regulator implicated in MYC function is the SWI/SNF chromatin remodeling complex, which is a large multi-subunit complex that uses the energy of ATP hydrolysis to alter contacts between histones and DNA (3, 4). Spurred on by cancer genome sequencing studies indicating that SWI/SNF subunits are mutated in ~20% of cancers (5, 6), the last several years have been marked by numerous impactful discoveries (7–11). Interestingly, almost all of these findings have been grounded in studies of malignant rhabdoid tumors (MRT) (7, 8, 10, 11), a malignancy in which the gene that encodes the SNF5 subunit of the SWI/SNF complex, *SMARCB1*, is lost (12). Reintroduction of SNF5 into MRT cell lines has revealed that SNF5 acts as a potent tumor suppressor through multiple mechanisms including maintaining enhancer activation (7, 8, 13), opposing polycomb complex function at bivalent promoters (7), and regulating the formation and function of a BRD9-marked non-canonical BAF (ncBAF, also known as GBAF (14)) (10, 11) complex.

In addition to its roles within SWI/SNF, SNF5 binds directly to the carboxy-terminus of MYC (15) where it was originally thought to act as a co-activator of MYC-dependent transcription. In contrast to that notion, we and others showed that SNF5 inhibits MYC function through tempering the ability of MYC to bind chromatin (16, 17) resulting in decreased target gene transcription (17). This revised understanding of the significance of the MYC-SNF5 interaction implies that loss of SNF5 in MRT results in unrestricted MYC function and explains how MYC target gene signatures are activated across SNF5-null cancers (18–20). More importantly, these data implicate MYC as a key driver of pro-tumorigenic transcriptional programs in MRT and suggest that MYC inhibitors, when available, could be used to treat SNF5-null cancers.

Beyond SNF5, however, it is unknown whether MYC can interact with additional SWI/SNF subunits. Here, we report that MYC uses multiple interaction surfaces to interact with SWI/SNF subunits independently of SNF5. We show that MYC interacts with the pan-SWI/SNF subunit, BAF155, and that almost all of MYC co-localizes with SWI/SNF subunits on chromatin in the MRT setting. Interaction of MYC with BAF155 is blocked by SNF5, indicating that, in addition to inhibition of DNA binding, SNF5 may also function by impeding access of MYC to other SWI/SNF subunits. Comprehensive analysis of MYC transcriptional activities in MRT cells shows that acute removal of MYC causes widespread gene expression changes and down-regulation of MYC-SWI/SNF target gene without corresponding changes in the open chromatin state. Our data reveal multiple mechanisms of MYC inhibition by SNF5 and highly suggest that MYC uses residual SWI/SNF proteins to effect transcriptional programs in MRT cells. This study lays a foundation from which to interrogate the influence of SWI/SNF on MYC function in cancers that show alterations to either SWI/SNF subunits or deregulation of MYC.

Results

MYC does not require SNF5 to interact with SWI/SNF.

To begin to unravel the interactions of MYC with SWI/SNF, we turned to HEK293 cells which express all characterized SWI/SNF complexes (10) and where we could easily manipulate MYC or MYC fragment expression (21, 22). Expression and immunoprecipitation of full-length (FL) Flag-tagged MYC revealed that MYC interacts with multiple SWI/SNF subunits, including SNF5 and the ncBAF subunit member, BRD9 (Fig. 1a), which is mutually exclusive with SNF5 within SWI/SNF complexes (10, 11). To eliminate contributions from SNF5, which binds to the carboxy-terminus of MYC (15), we also analyzed the central portion of MYC (CP: amino acids 151-319) fused to the Gal4-HA-flag DNA binding domain (21). As expected, the CP of MYC does not bind SNF5, although it robustly associates with several SWI/SNF subunits including BRD9 (Fig. 1a), suggesting that MYC is capable of interactions with SWI/SNF that do not require SNF5. To test this idea, we depleted SNF5 in HEK293 cells using the dTAG approach (17), and probed for its impact on interaction of MYC with BAF155—a subunit that is incorporated into all SWI/SNF complexes known to date (4). Again, the MYC–BAF155 interaction is largely insensitive to SNF5 depletion (Fig. 1b), revealing that MYC can associate with BAF155 even in the absence of SNF5.

We hypothesized that if MYC does not require SNF5 for all SWI/SNF interactions, it should interact with residual SWI/SNF subunits in MRT cells. Indeed, following IP of endogenous BAF155 in two MRT cell lines, G401 and A204, we found that BAF155 associates with MYC (Fig. 1c,d). We confirmed this association using proximity ligation assays (PLA): In A204 cells the number of MYC-BAF155 foci per nucleus is significantly larger than background MYC or BAF155 foci alone (Fig. 1e,f). Similar results were obtained from assays in G401 cells (Fig. 1g,h). These results are consistent with the HEK293 cell data and provide compelling evidence that MYC associates with SWI/SNF subunits without requiring any interaction with SNF5.

MYC co-localizes with multiple SWI/SNF subunits on chromatin in MRT cells at promoters.

Recently, we discovered that MYC function is required for multiple aspects of MRT biology (17). Our discovery that MYC can interact with SWI/SNF in a SNF5-independent manner raises the possibility that MYC might be working with residual SWI/SNF subunits in MRT cells to drive an oncogenic transcriptional program. To determine the extent of MYC and SWI/SNF interactions on chromatin in this setting, we compared ChIP-seq data for MYC performed in G401 cells (GSE109310, (17)) to publicly available ChIP-seq datasets for the SWI/SNF ATPase BRG1 (GSE90634, (7)), pan-subunit BAF155 (GSE90634, (7)), and the exclusive non-canonical BAF subunit, BRD9 (GSE120235, (11)). Intriguingly, ~96% of detected MYC binding sites co-localize with at least one subunit of SWI/SNF, and ~70% of MYC co-localizes with both BRG1 and BAF155 (Fig. 2a). About half of the sites in which MYC, BRG1, and BAF155 co-localize are also marked by BRD9, revealing at least two types of MYC-SWI/SNF interactions on chromatin: MYC/BRG1/BAF155 (Supplementary Fig. 1a, **top**) and MYC/BRG1/BAF155/BRD9 (Supplementary Fig. 1a, **bottom**). The presence of BRD9 on chromatin does not correlate with altered intensity of MYC binding

(Fig. 2b) nor do we find that presence of MYC significantly influences the ChIP-seq signal for BRD9 (Fig. 2c), which is distinct from non-MYC BRG1/BAF155 overlapped peaks (Supplementary Fig. 1c).

Separating MYC-BRG1-BAF155 co-bound sites (collectively referred as “MYC-SWI/SNF” herein) based on distance from nearest transcription start site (TSS) reveals that these sites are predominantly promoter proximal (Fig. 2d). Further comparison of MYC-SWI/SNF peaks with promoters defined by peaks marked by histone H3 lysine 4 tri-methylation (H3K4me3) and histone H3 lysine 27 acetylation (H3K27ac) that fall within 1 kb of the nearest TSS revealed that ~80% of MYC-SWI/SNF peaks are found at promoters (Fig. 2e). This is in contrast to overlap with enhancers regions marked by H3K27ac without H3K4me3, and are defined by peaks that are more than 1 kb from TSS (Fig. 2f). Strikingly, areas of MYC-SWI/SNF binding show a more than two-fold increase in H3K4me3 and H3K27ac binding compared to BRG1-BAF155 peaks without MYC and contain less of the enhancer associated histone H3 lysine 4 mono-methylation (H3K4me1) mark (Fig. 2g). Taken together our data reveal that the MYC-SWI/SNF association is overwhelmingly localized to promoter regions and may thus represent an additional SWI/SNF driven mechanism in MRT apart from enhancer regulation (7, 8).

Finally, we performed gene ontology (GO) enrichment analysis (<https://david.ncifcrf.gov/>) on genes within 1 kb of the TSS for MYC/BRG1/BAF155 or MYC/BRG1/BAF155/BRD9 peaks. Importantly, many of the core functions of MYC are captured in the genes associated with MYC-SWI/SNF, regardless of BRD9 presence (Supplementary Table 1, Fig. 2h,i). Separation of the two groups of genes revealed some overlapping biological functions but also unique functions, such as mitochondrion for MYC/BRG1/BAF155/noBRD9 target genes (Fig. 2h) or cell-cell adhesion and protein targeting for MYC/BRG1/BAF155/BRD9 target genes (Fig. 2i). Overall, we conclude that in MRT cells MYC shows extensive interactions on chromatin with multiple subunits of SWI/SNF and that MYC-SWI/SNF interactions in MRT take place at distinct sets of genes linked to core functions of MYC.

BAF155 is present at MYC-SWI/SNF bound sites in other tumor cell types.

The identification of MYC with SWI/SNF on chromatin independently of SNF5 prompted us to ask if SWI/SNF components are present at these sites in other SWI/SNF altered cancers. Given that the MYC-SWI/SNF target genes we identified are highly conserved MYC targets likely to be present in a majority of cancers (23) we asked if the core SWI/SNF component, BAF155, was also bound to these same sites. Initially we focused our comparisons on three synovial sarcoma (SS) cell lines: Aska, HSSY2, and SYO1. SS cancers are driven by SS18-SSX fusion proteins which when incorporated into the SWI/SNF complex result in eviction and subsequent degradation of SNF5 (24), making these cancers SNF5-deficient. Comparing detected BAF155 peaks with MYC-SWI/SNF peaks in G401 cells revealed that the majority (~69-95%) of MYC-SWI/SNF peaks in MRT overlap with BAF155 peaks in these contexts (Fig. 3a, Supplementary Fig. 1c-e), suggesting that SWI/SNF components are preserved at conserved MYC sites. Next, to relate our findings to additional cancer settings, we compared binding of MYC-SWI/SNF to BAF155 detected in BRG1-deficient small cell carcinoma of the ovary, hypercalcemic type (SCCOHT), which

like MRT is both rare and aggressive and tumorigenesis has been linked directly to multiple mechanisms resulting from loss of a single SWI/SNF subunit (25, 26). Remarkably, almost all MYC-SWI/SNF peaks in MRT overlap with chromatin-bound BAF155 that remains following BRG1 loss in the SCCOHT cell line, BIN67, (Fig. 3b, Supplementary Fig. 1f). Comparison of a common set of BAF155 peaks identified across all four SWI/SNF altered cancer lines (Fig. 3c) to MYC-SWI/SNF peaks in MRT shows that over 60% of these sites are positive for BAF155 binding in other cell lines (Fig. 3d,e), indicating that across various cancers that show SWI/SNF alterations, a core SWI/SNF component is retained on chromatin at conserved MYC regions.

MYC binds the SWIRM domain of BAF155.

Besides SNF5 no other interactions of MYC with SWI/SNF components have been reported. To expose additional interactions between MYC and SWI/SNF, we began by characterizing further the interaction of MYC with BAF155. We expressed the MYC transcriptional activation domain, the DNA-binding domain, the CP, or various central portion truncation mutants, recovered them by Flag IP, and probed for BAF155. BAF155 interacts predominantly with the CP of MYC (Supplementary Fig. 2a), and is dependent on a region directly adjacent to the well-conserved MYC box IV (**see diagram**, Supplementary Fig. 2a).

BAF155 is known to make various interactions through its four major annotated domains (Supplementary Fig. 2b) (27–31). To uncover which of these domains is responsible for interaction with the MYC CP, we performed BAF155 domain mapping studies (Supplementary Fig. 2b). Immunoprecipitation experiments showed that the SWIRM domain of BAF155 is both necessary and sufficient for MYC binding (Fig. 4a). As previously observed (29), the SWIRM domain is also sufficient for endogenous SNF5 binding, although binding of SNF5 binding is more robust with full-length BAF155. Interestingly, full-length BAF170, which is 62% identical and 77% similar to BAF155 (32), associates with SNF5 but does not bind MYC, even though the isolated BAF170 SWIRM associates with MYC as well as that of BAF155 (Supplementary Fig. 2c). We conclude that the SWIRM domains of BAF155 and BAF170 mediate interaction with the CP of MYC, but that BAF170 SWIRM is likely not as accessible within the context of the full-length protein as that of BAF155.

We next asked if the SWIRM domain of BAF155 interacts directly with the MYC CP. We expressed and purified recombinant Sumo-tagged SWIRM (amino acids 417–580 of BAF155), Sumo-flag-tagged MYC CP (amino acids 151–319 of MYC), or Sumo protein as a control. Flag-IP for MYC recovered the SWIRM domain, but not Sumo alone (Fig. 4b), indicating that MYC and the BAF155 SWIRM domain can interact directly. We then compared SNF5-SWIRM interactions to MYC-SWIRM interactions and found that the SWIRM fragment binds SNF5 with an apparent higher affinity than MYC, and is dependent on residues 533–546 of the SWIRM domain (Supplementary Fig. 2d). Some, but not all, of the MYC binding is lost upon deletion of amino acids 533–546 (Supplementary Fig. 2d,e), but these residues are not sufficient for binding to either MYC or SNF5 (Fig. 4c), suggesting that the interactions are likely dependent on SWIRM structure as well as amino acid sequence. We then introduced two mutations (L534A, N536A, “AA”) shown to be critical

for the murine SNF5-SWIRM interaction (29) (Supplementary Fig. 2f) and found that they are highly effective at eliminating SNF5 binding, and partially effective at doing so to MYC (Fig. 4d), consistent with the idea that MYC and SNF5 use common and distinct regions of the SWIRM domain to mediate binding.

Based on their shared use of the SWIRM domain, we asked if MYC and SNF5 compete for binding to the BAF155 SWIRM domain. We saw that at a 1:1 molar ratio SNF5 is able to reduce the amount of MYC bound to the SWIRM domain (Fig. 4e), suggesting that when SNF5 is present, access of MYC to the BAF155 SWIRM may be inhibited. To test this idea, and validate our *in vitro* findings in cells, we expressed a T7-tagged wild-type SWIRM domain of BAF155 or the “AA” mutant in cells and probed for endogenous SNF5 or MYC following T7-IP. The AA SWIRM mutant impacts SNF5 binding as expected, albeit to lesser extent than in the purified system. MYC binding, in contrast shows an opposite increase in binding (Fig. 4f). Finally, we created small C-terminal deletions to target the SWIRM region within a fragment of BAF155 (amino acids 2–580) and co-expressed these with Flag-tagged full-length MYC. Here, removal of SNF5 binding through deletion of amino acids 533–580 causes a dramatic increase in full-length MYC binding (Fig. 4g). Consistent with our *in vitro* results pointing to MYC being able to access multiple regions of the SWIRM domain, MYC binding remained across all BAF155 truncation mutants. Taken together, these data reinforce the discovery of BAF155 as a novel and direct MYC-SWI/SNF interaction partner and suggest that SNF5 can temper the ability of MYC to bind BAF155.

MYC binds to chromatin for a non-chromatin remodeling function.

If SNF5 can temper the interaction of MYC with BAF155, it is possible that in MRT MYC has unlimited access to BAF155, potentially explaining the co-localization of MYC with SWI/SNF that we identified in G401 cells (Fig. 2a). Given that we have previously shown that MRT cells are dependent on MYC for multiple aspects of their biology (17), we decided that a comprehensive assessment of MYC transcriptional activities was warranted to fully understand MYC function in this malignancy. To assess early changes specific to MYC, we first engineered G401 cells, which we refer to as “DTMYC G401”, to express lentivirally-encoded c-MYC containing a N-terminal HA-FKBP12^{F36V} dTAG module and deleted endogenous c-MYC through CRISPR-Cas9 (Fig. 5a). In these cells, depletion of MYC by addition of a dTAG47 molecule was accomplished within four hours (Fig. 5b), allowing us much more acute control of MYC than our previous use of inducible OmoMYC system (17).

To identify sites of MYC binding that respond to its depletion, we performed chromatin immunoprecipitation coupled to next-generation sequencing (ChIP-seq) using antibodies against the HA-tag of MYC. We detected ~1250 peaks in these experiments, similar to the number of binding sites for endogenous MYC we reported previously (17). Treatment with dTAG47 for 4 hr results in a global decrease of MYC binding (Fig. 5c, Supplementary Fig. 3a), with 958 MYC binding sites being significantly down-regulated at this time point (Supplementary Table 2). Moreover, tagged MYC in DTMYC G401 cells displays authentic patterns of binding, as motif enrichment analysis identified the E-box motif, “CACGTG” (Supplementary Fig. 3b), the majority of MYC detected is promoter-proximal (Supplementary Fig. 3c), and the dTAG-sensitive genes are enriched within the canonical

functions of MYC (Supplementary Fig. 3d). Comparison of MYC targets detected in DTMYC G401 cells with MYC-SWI/SNF target genes (Supplementary Table 1) showed that over half of MYC-SWI/SNF targets identified in G401 cells are detected in our engineered cell line (Fig. 5d) and almost half are responsive to dTAG47 addition (Fig. 5e). Again, about half of all MYC-SWI/SNF target genes identified were marked by BRD9 (Supplementary Fig. 3e).

Next, we asked if depletion of MYC results in changes in the open chromatin state by assaying for transposase accessible chromatin followed by next-generation sequencing (ATAC-Seq) (17, 33) at 24 hr post dTAG47 treatment. Overall, we detected ~30,000 sites of open chromatin in DMSO-treated cells and ~80% of those sites were also identified in dTAG47-treated cells (Fig. 5f). Globally there were no significant changes in either direction following MYC depletion (Fig. 5g) and comparison of fold-changes obtained for ChIP-seq to overall fold-changes for ATAC-Seq (Fig. 5h) confirmed that there is no correlation between the presence of MYC on chromatin (including sites of MYC-SWI/SNF co-localization) and alterations in chromatin accessibility. We conclude that, in these MRT cells, MYC does not actively maintain the open chromatin state of MYC-bound genes.

MYC loss causes decreased MYC-SWI/SNF target gene expression.

To understand the role of MYC in regulating transcription in MRT cells, and in particular the role that MYC plays transcriptionally at MYC-SWI/SNF target genes, we performed RNA-seq in DTMYC G401 cells treated with either dTAG47 or DMSO control for 24 hr, a time point that MYC was maximally depleted (Fig. 6a). Overall, there are ~4,200 gene expression changes between the two treatments (Supplementary Table 3, Supplementary Fig. 4a). These changes are specific to MYC depletion, as RNA-seq performed on parental G401 cells treated with dTAG47 at the same time point did not reveal broad changes in transcript levels (Supplementary Fig. 4b). Only 15 transcripts are significantly changed in parental cells; all are up-regulated, and only 5 of which change in the same direction with degradation of MYC (Supplementary Fig. 4c). This result indicates that removal of MYC by the dTAG method is highly specific in this context. Comparison of MYC binding sites that lost MYC upon dTAG47 addition (Fig. 5c) to transcriptional changes revealed that genes with down-regulated MYC binding (FDR < 0.5 and greater than 2-fold change, Fig. 6b) or FDR < 0.5 only, Fig. 6c) are enriched among the down-regulated transcripts. Analysis of up-regulated transcripts revealed enrichments among several GO categories relating to movement and migration, signaling, and blood development (Fig. 6d). Gene set enrichment analysis (GSEA) using MSigDB Hallmark datasets showed hallmark MYC targets are enriched among the down-regulated transcripts (Supplementary Fig. 4d) and that hallmarks relating to epithelial-mesenchymal transition and coagulation are significantly enriched among up-regulated transcripts (Fig. 6e). In addition, gene sets corresponding to E2F targets (Supplementary Fig. 4d), MTORC1 signaling, and G2M checkpoint are enriched among down-regulated transcripts and KRAS signaling, apoptosis, and apical junction were enriched among up-regulated transcripts (Supplementary Table 4), indicating that loss of MYC in G401 cells results in diverse gene expression changes.

To examine primary transcriptional changes associated with MYC loss, we performed precision nuclear run-on assay coupled to next-generation sequencing (PRO-Seq) at 4 hr post-dTAG47 addition. Quantification of RNA polymerase density within gene bodies showed that MYC loss results in more genes having a decrease in RNA polymerase within the gene bodies than an increase (Fig. 6f, Supplementary Fig. 4e, Supplementary Table 5), and fold-changes are slightly larger for those with decreased gene body densities (Fig. 6g). GO-term analysis of genes with decreased gene body density showed enrichment among core functions of MYC (Supplementary Fig. 4f) and, consistent with our RNA-seq results, MYC binding sites that were down-regulated by dTAG47 addition as determined by ChIP-seq (FDR < 0.5) are enriched among those genes that experience a loss in gene body associated RNA polymerase (Fig. 6h). Direct comparison of genes impacted in PRO-Seq to RNA-seq changes showed that ~77% of genes with decrease in transcription at 4 hr are also down-regulated at the transcript level, while 63% of genes with increased transcription are up-regulated at the transcript level (Fig. 6i). Taken together, these data reinforce our previous findings that MYC is a prominent regulator of MRT gene expression programs and that MYC generally acts as a direct activator of MYC target gene expression in MRT cells.

Finally, we specifically focused on targets of MYC-SWI/SNF that respond to dTAG47 addition (Fig. 5e). Examining the impact of MYC loss on MYC-SWI/SNF target gene expression revealed that expression of ~61% of MYC-SWI/SNF targets are down-regulated by removal of MYC compared to only 2% being up-regulated (Fig. 7a), indicating that the majority of MYC-SWI/SNF targets are regulated positively by MYC. Importantly, these transcriptional effects appear to be due to primary actions of MYC on transcription, as PRO-Seq also detected a similar pattern of regulation (Fig. 7b) and almost all early transcriptional changes detected by PRO-Seq at MYC-SWI/SNF target genes persisted in the RNA-seq analysis (Fig. 7c). Overall comparison of the MYC-SWI/SNF associated transcripts that are down-regulated by RNA-seq to both PRO-Seq and ChIP-seq revealed that MYC is removed from chromatin at these MYC-SWI/SNF target genes, of which about half experience changes in transcription within hours upon MYC loss (Fig. 7d). The fold-change in gene expression specific to these targets is modest but consistent (Fig. 7e), suggesting that MYC—and potentially BRG1 and BAF155—function to maintain and modulate maximum gene expression at these sites.

Discussion

The past several years have witnessed a revolution in our understanding of the structure and functions of SWI/SNF chromatin remodeling complexes (7, 8, 10, 11, 13, 31, 34) with the SNF5 subunit of SWI/SNF being the center of key studies that have exposed the mechanisms by which SWI/SNF can function as a tumor suppressor. One such mechanism is that SNF5 works to antagonize MYC binding to chromatin, ultimately influencing the ability of MYC to recruit RNA polymerase for MYC-dependent transcription (17). In this study, we provide a comprehensive analysis of MYC activities in MRT. In addition, we find that MYC does not require SNF5 to interact with additional SWI/SNF subunits and that SNF5 may work to modulate the association of MYC with specific SWI/SNF subunits.

The evidence that MYC does not require SNF5 to interact with SWI/SNF is most apparent in our biochemical/cellular findings (Fig. 1) and genomic analyses that define MYC-SWI/SNF localization (Fig. 2). We find that the colocalization of MYC with BRG1 and BAF155 on chromatin in MRT occurs predominantly at promoter regions (Fig 2d–g), which is distinct from multiple studies that have focused on SWI/SNF regulation of enhancers (7, 8) or super-enhancers that are retained to maintain the tumor state (8). The presence of SWI/SNF at core MYC target genes is not limited to MRT as we found BAF155 bound at these same locations across various cancers showing SWI/SNF alteration (Fig. 3). Thus, our findings highlight a novel role for SWI/SNF at conserved MYC target gene promoters and support our recently proposed model of dual regulation (17) in which SNF5 can regulate distinct chromatin events at both TSS-proximal MYC promoters and TSS-distal enhancer sites. Interestingly, about half of MYC-SWI/SNF target genes identified in G401 cells are marked by the non-canonical BRD9 subunit of SWI/SNF (Fig. 2a), suggesting that there may be more than one type of SWI/SNF complex that MYC access. In HEK293T cells, MYC interacts with the ncBAF complex member BRD9 (Fig. 1a) and employs separate interaction surfaces to mediate specific SWI/SNF subunit interactions (Fig. 1a, Supplementary Fig. 2a). The only known SNF5-null SWI/SNF complex is the BRD9-containing ncBAF complex and it is intriguing to speculate that since this complex lacks SNF5, MYC interaction with ncBAF may function to drive and/or maintain MYC-target gene transcription.

But how can MYC gain access to multiple versions of a large, multi-subunit complex like SWI/SNF? We suspect that MYC may be able to use a subunit present in all SWI/SNF complexes characterized—BAF155. The evidence that MYC can specifically interact with BAF155 is compelling (Fig. 4), and consistent with evidence that BAF155 homodimers serve an early SWI/SNF intermediate through which additional SWI/SNF subunits, including SNF5, can then assemble (31), potentially providing opportunities for the complex to interact with non-SWI/SNF proteins such as MYC.

A detailed molecular analysis of the MYC-BAF155 interaction, revealed that MYC can directly bind the well-conserved SWIRM domain of BAF155, a region known to bind SNF5 (Fig. 4d). Data comparing MYC and SNF5 binding properties suggests that while MYC makes multiple interactions across the SWIRM sequence, a large portion of binding for MYC, and all binding for SNF5, occurs within the last 14 residues of the SWIRM domain (amino acids 533–546)—although that region alone is insufficient for binding. Intriguingly, MYC and SNF5 appear to compete for binding to the SWIRM domain of BAF155 (Fig. 4e–g). This is reminiscent of reports that BRD9 and SNF5 compete for access to SWI/SNF subunits (11), although it is unclear in those studies precisely how the competition is occurring. It is possible that, like MYC, BRD9 uses a common domain specific to one of the pan-SWI/SNF subunits to mediate the competition with SNF5. For both MYC and BRD9 (11) however, the presence of SNF5 appears to dominate in terms of apparent affinity for SWI/SNF subunit members, creating multiple ways in which SNF5-loss may lead to increased aberrant transcription once SNF5-dependent regulation is missing. As it relates specifically to MYC, these results suggest that in a cell in which SNF5 is present the MYC-BAF155 interaction is tempered by SNF5, shuttling MYC to the inhibitory MYC-SNF5 interaction (17).

We posit that the MYC-SWI/SNF interaction in MRT is not inhibitory but instead serves to stimulate MYC-driven transcription. Although more work needs to be done, we did provide a solid framework in which to interrogate the MYC-SWI/SNF interaction in future studies. Using the dTAG approach we were able to modulate MYC much more rapidly than in our previous studies using OmoMYC (17). Using this system, we found that MYC binding does not impact the open chromatin state (Fig. 5f), at least at the time point we examined, suggesting that SWI/SNF complexes present following SNF5 loss may not function in chromatin remodeling or MYC may not recruit SWI/SNF to these sites. The combination of RNA-seq and PRO-Seq in this study allow us an unprecedented view of the influence of MYC in MRT, of which we did not have previously. We saw changes in MYC target gene expression, and specifically MYC-SWI/SNF target gene expression (Fig. 6, 7), are predominately due to changes in transcription itself indicating that MYC chiefly acts as a direct activator of MYC-SWI/SNF target gene expression in MRT. Identification of the MYC-SWI/SNF target genes in MRT cells and how they respond to changes in MYC is the first step in the direction of uncovering the precise role that SWI/SNF plays on MYC-dependent transcription. Building on these results and expanding the findings to other cancers in which SWI/SNF and/or MYC are mutated will be critical in future studies.

Materials and Methods

Cell culture and transductions.

All cell lines were obtained from ATCC as previously noted (17), except HEK293T cells which are in-house stocks. All HEK293 and G401 cells were maintained in DMEM with 10% fetal bovine serum (FBS) and 1% Penicillin/Streptomycin while A204 cells were maintained in RPMI with 10% FBS and 1% Penicillin/Streptomycin, respectively. Lentiviral transductions were performed by transfecting HEK293 cells with the DTMYC construct (described below), along with the pMD2.G and the psPAX2 packaging plasmid. pMD2.G was a gift from Didier Trono (Addgene plasmid # 12259 ; <http://n2t.net/addgene:12259> ; RRID:Addgene_12259) and psPAX2 was a gift from Didier Trono (Addgene plasmid # 12260 ; <http://n2t.net/addgene:12260> ; RRID:Addgene_12260). Viral supernatant collected in maintenance media was used to infect G401 cells. Transductions took place over two days and then cells were allowed to recover for one day prior to selection with 1 µg/ml puromycin.

Proximity ligation assay.

Coverslips were pretreated with poly D-lysine, and then cells were plated onto coverslips at sub-confluence. Cells were fixed in 4% methanol-free formaldehyde for ten minutes and permeabilized with 0.5% Triton for ten minutes. Proximity ligation assays were performed with the Duolink PLA mouse/rabbit kit (*Sigma*) according to the manufacturer's instructions. Nuclei were stained using Duolink in situ mounting medium with DAPI (*Sigma* DUO82040). Primary antibodies used were mouse anti-MYC (*Santa Cruz* c33) and rabbit anti-BAF155 (*Abcam* ab72503). Confocal images were acquired using an Andor DU-897 EMCCD camera mounted on a Nikon Spinning Disk Microscope. Fluorescent puncta were quantified by using FIJI (ImageJ) to calculate the number of maxima within each nucleus.

Plasmids for generation of DTMYC G401 cells.

To target endogenous MYC using CRISPR, an oligo containing one guide sequence against MYC (GCCGTATTTCTACTGCGACG), was annealed, phosphorylated, and then inserted into the pSpCas9(BB)-2A-GFP (PX458) vector (35). To engineer a lentiviral construct to express a version of MYC that could be degraded by dTAG47 addition, DNA sequences encoding full-length MYC were PCR amplified from pFlag-MYC (21) and inserted into the multiple cloning site of pENTR1A (17, 36) via Gibson assembly. The PAM sequence recognized by the engineered Cas9-sgRNA vector was then destroyed using whole plasmid mutagenesis to induce silent mutations. Sequences encoding this form of MYC was then inserted in frame into the lentiviral pLEX-305-N-dTAG vector (17, 37) using gateway cloning (*Life Technologies*). All plasmid sequences were confirmed by DNA sequencing. pSpCas9(BB)-2A-GFP (PX458) was a gift from Feng Zhang (Addgene plasmid # 48138 ; <http://n2t.net/addgene:48138> ; RRID:Addgene_48138). pENTR1A no ccDB (w48-1) was a gift from Eric Campeau & Paul Kaufman (Addgene plasmid # 17398 ; <http://n2t.net/addgene:17398> ; RRID:Addgene_17398). pLEX_305-N-dTAG was a gift from James Bradner (Addgene plasmid # 91797 ; <http://n2t.net/addgene:91797> ; RRID:Addgene_91797).

Additional plasmid construction.

Plasmids encoding Gal4, Flag- and HA- epitope tagged central portion, the transcriptional activation domain, or the DNA-binding domain of MYC were created previously (21). Whole-plasmid mutagenesis of the central portion of MYC with Q5 polymerase (*New England BioLabs*) was used to create any truncations or deletion constructs. For all T7-tagged BAF155 constructs, sequences corresponding to the appropriate region of BAF155 were amplified out pFastBac1 Flag BAF155 b (38) to encode a C-terminal 3X SV40 nuclear localization sequence and inserted into a pCGT vector (39). To create similar constructs for BAF170, the plasmid pFastBac1 Flag BAF170 (38) was used as the source for all amplified sequences. pFastBac1 Flag BAF155 b was a gift from Robert Kingston (Addgene plasmid # 1954; <http://n2t.net/addgene:1954>; RRID:Addgene_1954). pFastBac1 Flag Baf170 was a gift from Robert Kingston (Addgene plasmid # 1955 ; <http://n2t.net/addgene:1955> ; RRID:Addgene_1955).

Creation of DTMYC G401 cell line.

G401 cells were transduced with the lentiviral vector containing MYC with an upstream HA-epitope tag-FKBP dTAG module (see “plasmid generation” in above methods). Following selection using puromycin, G401 cells were transfected with a single pX458 Cas9-GFP expression vector containing a guide RNA against MYC using Lipofectamine 3000 (*Life Technologies*), following the manufacturer’s protocol. After 3 days, cells were harvested, filtered through a 35 µm nylon mesh Falcon round bottom test tube, and then delivered to the Vanderbilt Flow Cytometry Shared Resource for single-cell sorting on a BD FACSAria III instrument. Clones obtained were analyzed to identify cell lines that retained exogenous expression of DT-MYC as the sole form of MYC present.

Production of recombinant proteins.

The region of MYC encompassing amino acids 151–319 was amplified from a pFLAG-MYC construct (21), along with a Flag-epitope tag, and inserted into a pSUMO expression vector (21). For SNF5, SNF5 coding sequences were amplified from a pFASTBac1 INI1 construct (38) to include a Flag-epitope and inserted into pSUMO. pFastBac1 INI1 was a gift from Robert Kingston (Addgene plasmid # 1953 ; <http://n2t.net/addgene:1953> ; RRID:Addgene_1953). The SWIRM domain encompassing amino acids 417–580 of BAF155 were amplified from pFASTBac1 BAF155 vector described above and inserted into pSUMO as well. These constructs were modified to create truncations or mutants using whole-plasmid mutagenesis with Q5 polymerase (*NEB*). For the SWIRM 533–580 construct amino acids corresponding to that region of BAF155 were multimerized four times in a plasmid containing the appropriate restriction enzyme sites (*GenScript*) and inserted in pSUMO. All SUMO constructs including SUMO alone were transformed into Rosetta *E. coli* cells (*EMD Millipore*) and purified using a non-denaturing lysis buffer and Ni-NTA agarose, according to the Ni-NTA QIAGEN protocol (*Qiagen*). SNF5 and SWIRM domain protein expression were induced with IPTG overnight at 16°C, while the MYC central portion (Flag-MYC-CP) protein fragment and SUMO protein alone were induced for 3 hours at 37°C. Following elution in 1X PBS containing 250mM imidazole, 2mM DTT, and 10% glycerol, proteins were snap frozen in liquid nitrogen and stored at –80°C until ready for use.

Recombinant pull-down assays.

50 µg of Flag-MYC-CP or Flag-SNF5 was combined with 30 µg of appropriate SWIRM domain protein or SUMO protein alone. For competition assay, equimolar amounts of HA-MYC CP or untagged SNF5 were combined with 2 µg Flag-tagged SWIRM (417–564). Combined proteins were diluted in Lysis buffer (150 mM Tris-HCl pH 8.0, 150 mM NaCl, 5 mM EDTA, 1% Triton X-100, PMSF, with Protease Inhibitor Cocktail; *Roche*) and a fraction collected as “input”. Flag-tagged proteins were isolated by rotating with M2-agarose overnight at 4°C, followed by washing four times in Lysis buffer containing 300 mM sodium chloride. Flag proteins, along with any co-bound proteins, were eluted with 12 µg of 3X FLAG peptide (*Sigma Aldrich*) twice and elutions pooled. All proteins were resolved by SDS-PAGE and visualized by Coomassie Blue staining. Images were taken on a Bio-Rad gel doc.

Immunoprecipitation experiments.

For T7- and Flag-IP experiments, HEK293T cells were transiently transfected for 24 hr with indicated plasmids, along with GFP to tell transfection efficiency, using calcium phosphate transfection. Cells were lysed in Lysis Buffer, sonicated, and debris cleared by centrifugation. Equal amounts of lysates were used for immunoprecipitation with T7 antibody or, in the case of Flag-IP, M2-conjugated agarose beads (*Sigma*) overnight at 4°C. For T7-IPs, antibody complexes were bound to protein G agarose (*Sigma*) the next day. Following binding, all IP samples were washed extensively in Lysis Buffer and then boiled in loading dye. For endogenous BAF155 co-immunoprecipitation experiments, samples were processed similarly, except cells were treated for 1.5 hr with 25 µM MG132 (*VWR*)

and then nuclei from cells were extracted in 10mM HEPES, pH 7.9, 10mM KCl, 0.4% NP-40 prior to lysis in Lysis Buffer. Equal amounts of nuclear lysates were subjected to immunoprecipitation with 5 μ l of BAF155 antibody (*Cell Signaling*, 11956) overnight at 4°C and bound to protein A agarose (*Roche*) the next day. Following four washes as described above, samples were boiled in loading dye.

Western blotting and antibodies.

All proteins were resolved by SDS-PAGE and transferred to PVDF membrane (*PerkinElmer*) and blocked in 5% milk in TBS-T (50 mM Tris, pH 7.5, 150 mM NaCl, 0.1% Tween-20). The following antibodies were used in this study: T7 antibody (*EMD Millipore*, 69522–3), T7-HRP (*EMD Millipore*, 69048), Flag-HRP (*Sigma*, A8592 and *Cell Signaling*, 86861), SNF5 (*Bethyl Laboratories*, A301-087A, *Abcam*, ab12167, and *Cell Signaling*, 91735), BAF155 (*Cell Signaling*, 11956), GAPDH-HRP (*Cell Signaling*, 8884S), BAF170 (*Bethyl Laboratories*, A301-039A), BRG1 (*Cell Signaling*, 49360) HA-epitope tag (*Cell Signaling*, C29F4), HA-HRP (*Roche*, 12013819001), MYC (*Abcam*, ab32072), and BRD9 (*Active Motif*, 61537). Bands were visualized using Supersignal West Pico (*Pierce*) and traditional film development or using Clarity Western ECL substrate (*Bio-Rad*) in which a ChemiDoc MP (*Bio-Rad*) was used for development.

ChIP-Seq.

Approximately 10×10^6 DTMYC G401 cells per plate were treated with 500 nM dTAG47 or DMSO for 4 hours and processed for chromatin extraction. Generation of chromatin was performed as described previously (17). Briefly, following cross-linking the nuclei were extracted and chromatin was fragmented using a Diagenode Bioruptor. Immunoprecipitation was performed on chromatin from 10×10^6 cells using antibodies against HA-epitope (*Cell Signaling*, C29F4) or normal rabbit IgG control (*Cell Signaling*, 2729S). Immunoprecipitated DNA was bound to protein A agarose (*Roche*), washed extensively, and de-crosslinked overnight at 65°C as described previously (17). Chromatin from three ChIPs were combined and purified using with a PCR purification kit (*Qiagen*). Eluted DNA was then cleaned-up using AMPure beads and used to create libraries following the Ultra II DNA library Prep protocol with Multiplex Oligos for Illumina (*New England BioLabs*). Sequencing data were obtained on an Illumina NovaSeq 6000 with 150 bp paired end reads. Sequencing was performed by the Vanderbilt Technologies for Advanced Genomics (VANTAGE) Core at Vanderbilt University Medical Center.

ATAC-Seq.

DTMYC G401 cells were plated at 1×10^6 with either 500 nM dTAG47 or DMSO control for 24 hr and then 75,000 cells harvested as we have done previously (17). Libraries of transposed DNA were generated through PCR amplification at the cycle number determined to be optimal for each sample, using Nextera based primers (obtained from *IDT*) designed to allow for dual indexing of samples. Amplified libraries were submitted to the VANTAGE core at Vanderbilt for sequencing on an Illumina NovaSeq 6000 with 150 bp paired end reads following their ATAC-seq sequencing protocol.

RNA-seq.

1×10^6 DTMYC G401 cells were treated with 500 nM dTAG47 or DMSO control for 24 hr and RNA extracted using Direct-zol RNA mini prep kit (*Zymo*), which includes DNase treatment. 2 μ g of purified RNA was submitted to the VANTAGE core at Vanderbilt who handled ribosomal RNA depletion and production of libraries using their standard methods. Sequencing data was obtained on an Illumina NovaSeq 6000 with 150bp paired end reads.

PRO-Seq.

Approximately 30×10^6 DTMYC G401 cells were treated with 500 nM dTAG47 or DMSO and nuclei were harvested as described previously (17). Run-on reactions were performed using Biotin-11-CTP (*PerkinElmer*, NEL542001) for 3 minutes at 30°C and stopped by adding Trizol LS (*Thermo Scientific*). RNA was purified and extracted prior to undergoing a base hydrolysis. Streptavidin Dynabeads (*ThermoFisher*, 65601) were incubated with RNA and elution of bound RNA, adaptor ligations, and all steps of library creation were performed following our previous protocol (17). Amplified libraries were submitted to the VANTAGE core at Vanderbilt for sequencing on an Illumina NovaSeq 6000 with 150 bp paired end reads.

ChIP-Seq analysis.

Sequencing reads were aligned to the Hg19 human genome using Bowtie2 (40). MACS2 was used to call peaks with a q-value of 0.05 (41). Identification of consensus peaks for each sample was done using DiffBind (42) and peaks present in at least two replicates were included. The final peak set was produced using peaks identified across all samples and ChIP-seq read counts calculated. Normalization of reads was against total mapped reads, and differential peaks were determined using DESeq2 (43). Significantly changed peaks were determined using a FDR cut off of less than 0.05. Peaks were annotated using Homer annotatePeaks command line with default settings (<http://homer.ucsd.edu/homer/>) and motifs identified using Homer findMotifsGenome. Gene ontology analysis was performed using functional annotation clustering through DAVID (<https://david.ncifcrf.gov/>) on annotated peaks that fell within 1 kb of a transcription start site. The overlap of MYC peaks (GSE109310) with published BRG1(GSE90634), BAF155 (GSE90634), and BRD9 (GSE120235) were called as colocalized if peaks overlapped by at least one base pair. For BRD9, analysis of fastq files was performed using same methods as described above, using the overlapped peaks between both replicates as the final peak list for BRD9 binding sites used in this study. For BRG1 and BAF155, peak lists that were provided on GEO were used for the overlapping analysis. These additional published data sets were used in this manuscript: H3K4me3, H3K4me1 and H3K27ac (GSE71506) (8), BAF155 in Aska, SYO1, and HSSY2 (GSE108025) (24), and BAF155 in BIN67 (GSE117735) (25). Promoters were identified in G401 cells using regions that were positive for both H3K4me3 and H3K27ac that were within 1 kb of TSS, while enhancers were identified using that contained H3K27ac without H3K4me3 and were more than 1 kb away from any TSS.

ATAC-Seq analysis.

ATAC-seq sequencing data was aligned to the hg19 human genome and peaks called in each sample as in ChIP-seq analysis except adaptor sequences were trimmed prior to aligning using Cutadapt (44) (cutadapt -a CTGTCTCTTATACACATCT-minimum-length 15 -paired-output). Peaks were identified using DiffBind (42). Peaks present in at least two replicates per condition were included and the final peak set was produced using peaks identified across all samples with ATAC-seq read counts calculated. Differential peaks were identified using DESeq2 (43).

PRO-Seq analysis.

Following low quality sequencing removal and adaptor trimming (Cutadapt (44)), sequencing reads longer than 15 bp were reverse complimented with FastX tools and then aligned to the hg19 human genome using Bowtie2 (40). Any reads mapping to rRNA loci or having a mapping quality of less than 10 were removed. BAM files that were generated were feed into NRSA (<http://bioinfo.vanderbilt.edu/NRSA/>) to estimate RNA polymerase abundance in proximal-promoter and gene body regions of genes, to calculate pausing index and pausing index alterations, and to detect enhancers and quantify eRNA changes (45).

RNA-Seq analysis.

Following adapter trimming by Cutadapt (44), RNA-seq reads were aligned to the hg19 human genome using STAR (46) and quantified by featureCounts (47). Differential analysis were performed by DESeq2 (43), which determined the log2 fold changes, Wald test p-values, and adjusted p-value (FDR) by the Benjamini-Hochberg procedure. The significantly changed genes were assessed with a $FDR < 0.05$.

Supplementary Material

Refer to Web version on PubMed Central for supplementary material.

Acknowledgements

Special thanks to Dr. Scott Hiebert for his invaluable contributions. We would also like to thank the Vanderbilt University Medical Center Flow Cytometry Shared Resource, the Vanderbilt University Chemical Synthesis Core, the Vanderbilt Cell Imaging Shared Resource (CISR), and the Vanderbilt University Medical Center Technologies for Advanced Genomics (VANTAGE) Core for their critical assistance in this project. The Nikon Center of Excellence located in CISR is supported by NIH grants CA68485, DK20593, DK58404, DK59637, and EY08126. This work was supported by The Rally Foundation for Childhood Cancer Research Young Investigator Award and T32CA119925 to A.M.W, by the NIH/NCI, F31CA225065 and T32CA009582 to A.D.G, and grants from Alex's Lemonade Stand Foundation, St. Baldrick's Foundation, the Robert J. Kleberg and Helen C. Kleberg Foundation, and grant CA247833 from the NIH/NCI to W.P.T.

Data Availability.

All sequencing data have been deposited at GEO with the accession number GSE164926. All next-generation sequencing data metrics are shown in Supplementary Table 6. Any other data are available upon request.

References

1. Tansey WP. Mammalian MYC proteins and cancer. *New Journal of Science*. 2014;2013:1–27.
2. Thomas LR, Tansey WP. MYC and Chromatin. *The Open Access Journal of Science and Technology*. 2015;3:101124.
3. Hohmann AF, Vakoc CR. A rationale to target the SWI/SNF complex for cancer therapy. *Trends Genet*. 2014;30(8):356–63. [PubMed: 24932742]
4. Reddy D, Workman JL. Targeting BAF-perturbed cancers. *Nat Cell Biol*. 2018;20(12):1332–3. [PubMed: 30482940]
5. Kadoch C, Hargreaves DC, Hodges C, Elias L, Ho L, Ranish J, et al. Proteomic and bioinformatic analysis of mammalian SWI/SNF complexes identifies extensive roles in human malignancy. *Nat Genet*. 2013;45(6):592–601. [PubMed: 23644491]
6. Shain AH, Pollack JR. The spectrum of SWI/SNF mutations, ubiquitous in human cancers. *PLoS One*. 2013;8(1):e55119. [PubMed: 23355908]
7. Nakayama RT, Pulice JL, Valencia AM, McBride MJ, McKenzie ZM, Gillespie MA, et al. SMARCB1 is required for widespread BAF complex-mediated activation of enhancers and bivalent promoters. *Nat Genet*. 2017;49(11):1613–23. [PubMed: 28945250]
8. Wang X, Lee RS, Alver BH, Haswell JR, Wang S, Mieczkowski J, et al. SMARCB1-mediated SWI/SNF complex function is essential for enhancer regulation. *Nat Genet*. 2017;49(2):289–95. [PubMed: 27941797]
9. Gatchalian J, Malik S, Ho J, Lee DS, Kelso TWR, Shokhirev MN, et al. A non-canonical BRD9-containing BAF chromatin remodeling complex regulates naive pluripotency in mouse embryonic stem cells. *Nat Commun*. 2018;9(1):5139. [PubMed: 30510198]
10. Michel BC, D'Avino AR, Cassel SH, Mashtalir N, McKenzie ZM, McBride MJ, et al. A non-canonical SWI/SNF complex is a synthetic lethal target in cancers driven by BAF complex perturbation. *Nat Cell Biol*. 2018;20(12):1410–20. [PubMed: 30397315]
11. Wang X, Wang S, Troisi EC, Howard TP, Haswell JR, Wolf BK, et al. BRD9 defines a SWI/SNF sub-complex and constitutes a specific vulnerability in malignant rhabdoid tumors. *Nat Commun*. 2019;10(1):1881. [PubMed: 31015438]
12. Mittal P, Roberts CWM. The SWI/SNF complex in cancer - biology, biomarkers and therapy. *Nat Rev Clin Oncol*. 2020;17(7):435–48. [PubMed: 32303701]
13. Alver BH, Kim KH, Lu P, Wang X, Manchester HE, Wang W, et al. The SWI/SNF chromatin remodelling complex is required for maintenance of lineage specific enhancers. *Nat Commun*. 2017;8:14648. [PubMed: 28262751]
14. Alps A, Dykhuizen EC. Glioma tumor suppressor candidate region gene 1 (GLTSCR1) and its paralog GLTSCR1-like form SWI/SNF chromatin remodeling subcomplexes. *J Biol Chem*. 2018;293(11):3892–903. [PubMed: 29374058]
15. Cheng SW, Davies KP, Yung E, Beltran RJ, Yu J, Kalpana GV. c-MYC interacts with INI1/hSNF5 and requires the SWI/SNF complex for transactivation function. *Nat Genet*. 1999;22(1):102–5. [PubMed: 10319872]
16. Stojanova A, Tu WB, Ponzielli R, Kotlyar M, Chan PK, Boutros PC, et al. MYC interaction with the tumor suppressive SWI/SNF complex member INI1 regulates transcription and cellular transformation. *Cell Cycle*. 2016;15(13):1693–705. [PubMed: 27267444]
17. Weissmiller AM, Wang J, Lorey SL, Howard GC, Martinez E, Liu Q, et al. Inhibition of MYC by the SMARCB1 tumor suppressor. *Nat Commun*. 2019;10(1):2014. [PubMed: 31043611]
18. Gadd S, Sredni ST, Huang CC, Perlman EJ, Renal Tumor Committee of the Children's Oncology G. Rhabdoid tumor: gene expression clues to pathogenesis and potential therapeutic targets. *Lab Invest*. 2010;90(5):724–38. [PubMed: 20212451]
19. Wang X, Werneck MB, Wilson BG, Kim HJ, Kluk MJ, Thom CS, et al. TCR-dependent transformation of mature memory phenotype T cells in mice. *The Journal of clinical investigation*. 2011;121(10):3834–45. [PubMed: 21926465]
20. Genovese G, Carugo A, Tepper J, Robinson FS, Li L, Svelto M, et al. Synthetic vulnerabilities of mesenchymal subpopulations in pancreatic cancer. *Nature*. 2017;542(7641):362–6. [PubMed: 28178232]

21. Thomas LR, Wang Q, Grieb BC, Phan J, Foshage AM, Sun Q, et al. Interaction with WDR5 promotes target gene recognition and tumorigenesis by MYC. *Mol Cell*. 2015;58(3):440–52. [PubMed: 25818646]
22. Thomas LR, Foshage AM, Weissmiller AM, Popay TM, Grieb BC, Qualls SJ, et al. Interaction of MYC with host cell factor-1 is mediated by the evolutionarily conserved Myc box IV motif. *Oncogene*. 2016;35(27):3613–8. [PubMed: 26522729]
23. Ji H, Wu G, Zhan X, Nolan A, Koh C, De Marzo A, et al. Cell-type independent MYC target genes reveal a primordial signature involved in biomass accumulation. *PLoS One*. 2011;6(10):e26057. [PubMed: 22039435]
24. McBride MJ, Pulice JL, Beird HC, Ingram DR, D'Avino AR, Shern JF, et al. The SS18-SSX Fusion Oncoprotein Hijacks BAF Complex Targeting and Function to Drive Synovial Sarcoma. *Cancer cell*. 2018;33(6):1128–41 e7. [PubMed: 29861296]
25. Pan J, McKenzie ZM, D'Avino AR, Mashtalir N, Lareau CA, St Pierre R, et al. The ATPase module of mammalian SWI/SNF family complexes mediates subcomplex identity and catalytic activity-independent genomic targeting. *Nat Genet*. 2019;51(4):618–26. [PubMed: 30858614]
26. Orlando KA, Douglas AK, Abudu A, Wang Y, Tessier-Cloutier B, Su W, et al. Re-expression of SMARCA4/BRG1 in small cell carcinoma of ovary, hypercalcemic type (SCCOHT) promotes an epithelial-like gene signature through an AP-1-dependent mechanism. *eLife*. 2020;9.
27. Boyer LA, Langer MR, Crowley KA, Tan S, Denu JM, Peterson CL. Essential role for the SANT domain in the functioning of multiple chromatin remodeling enzymes. *Mol Cell*. 2002;10(4):935–42. [PubMed: 12419236]
28. Boyer LA, Latek RR, Peterson CL. The SANT domain: a unique histone-tail-binding module? *Nat Rev Mol Cell Biol*. 2004;5(2):158–63. [PubMed: 15040448]
29. Sohn DH, Lee KY, Lee C, Oh J, Chung H, Jeon SH, et al. SRG3 interacts directly with the major components of the SWI/SNF chromatin remodeling complex and protects them from proteasomal degradation. *J Biol Chem*. 2007;282(14):10614–24. [PubMed: 17255092]
30. Wang L, Zhao Z, Meyer MB, Saha S, Yu M, Guo A, et al. CARM1 methylates chromatin remodeling factor BAF155 to enhance tumor progression and metastasis. *Cancer cell*. 2014;25(1):21–36. [PubMed: 24434208]
31. Mashtalir N, D'Avino AR, Michel BC, Luo J, Pan J, Otto JE, et al. Modular Organization and Assembly of SWI/SNF Family Chromatin Remodeling Complexes. *Cell*. 2018;175(5):1272–88 e20. [PubMed: 30343899]
32. Wang W, Xue Y, Zhou S, Kuo A, Cairns BR, Crabtree GR. Diversity and specialization of mammalian SWI/SNF complexes. *Genes Dev*. 1996;10(17):2117–30. [PubMed: 8804307]
33. Buenrostro JD, Giresi PG, Zaba LC, Chang HY, Greenleaf WJ. Transposition of native chromatin for fast and sensitive epigenomic profiling of open chromatin, DNA-binding proteins and nucleosome position. *Nat Methods*. 2013;10(12):1213–8. [PubMed: 24097267]
34. Vierbuchen T, Ling E, Cowley CJ, Couch CH, Wang X, Harmin DA, et al. AP-1 Transcription Factors and the BAF Complex Mediate Signal-Dependent Enhancer Selection. *Mol Cell*. 2017;68(6):1067–82 e12. [PubMed: 29272704]
35. Ran FA, Hsu PD, Wright J, Agarwala V, Scott DA, Zhang F. Genome engineering using the CRISPR-Cas9 system. *Nat Protoc*. 2013;8(11):2281–308. [PubMed: 24157548]
36. Campeau E, Ruhl VE, Rodier F, Smith CL, Rahmberg BL, Fuss JO, et al. A versatile viral system for expression and depletion of proteins in mammalian cells. *PLoS One*. 2009;4(8):e6529. [PubMed: 19657394]
37. Nabet B, Roberts JM, Buckley DL, Paulk J, Dastjerdi S, Yang A, et al. The dTAG system for immediate and target-specific protein degradation. *Nat Chem Biol*. 2018;14(5):431–41. [PubMed: 29581585]
38. Phelan ML, Sif S, Narlikar GJ, Kingston RE. Reconstitution of a core chromatin remodeling complex from SWI/SNF subunits. *Mol Cell*. 1999;3(2):247–53. [PubMed: 10078207]
39. Wilson AC, Peterson MG, Herr W. The HCF repeat is an unusual proteolytic cleavage signal. *Genes Dev*. 1995;9(20):2445–58. [PubMed: 7590226]
40. Langmead B, Trapnell C, Pop M, Salzberg SL. Ultrafast and memory-efficient alignment of short DNA sequences to the human genome. *Genome Biol*. 2009;10(3):R25. [PubMed: 19261174]

41. Feng J, Liu T, Qin B, Zhang Y, Liu XS. Identifying ChIP-seq enrichment using MACS. *Nat Protoc.* 2012;7(9):1728–40. [PubMed: 22936215]
42. Stark RB, G.D. DiffBind: differential binding analysis of ChIP-seq peak data. *Bioconductor.* 2011. 10.1038/s41388-021-01804-7
43. Love MI, Huber W, Anders S. Moderated estimation of fold change and dispersion for RNA-seq data with DESeq2. *Genome Biol.* 2014;15(12):550. [PubMed: 25516281]
44. Martin M Cutadapt removes adapter sequences from high-throughput sequencing reads. *EMBnet journal.* 2011;17:10–2.
45. Wang J, Zhao Y, Zhou X, Hiebert SW, Liu Q, Shyr Y. Nascent RNA sequencing analysis provides insights into enhancer-mediated gene regulation. *BMC genomics.* 2018;19(1):633. [PubMed: 30139328]
46. Dobin A, Davis CA, Schlesinger F, Drenkow J, Zaleski C, Jha S, et al. STAR: ultrafast universal RNA-seq aligner. *Bioinformatics.* 2013;29(1):15–21. [PubMed: 23104886]
47. Liao Y, Smyth GK, Shi W. featureCounts: an efficient general purpose program for assigning sequence reads to genomic features. *Bioinformatics.* 2014;30(7):923–30. [PubMed: 24227677]

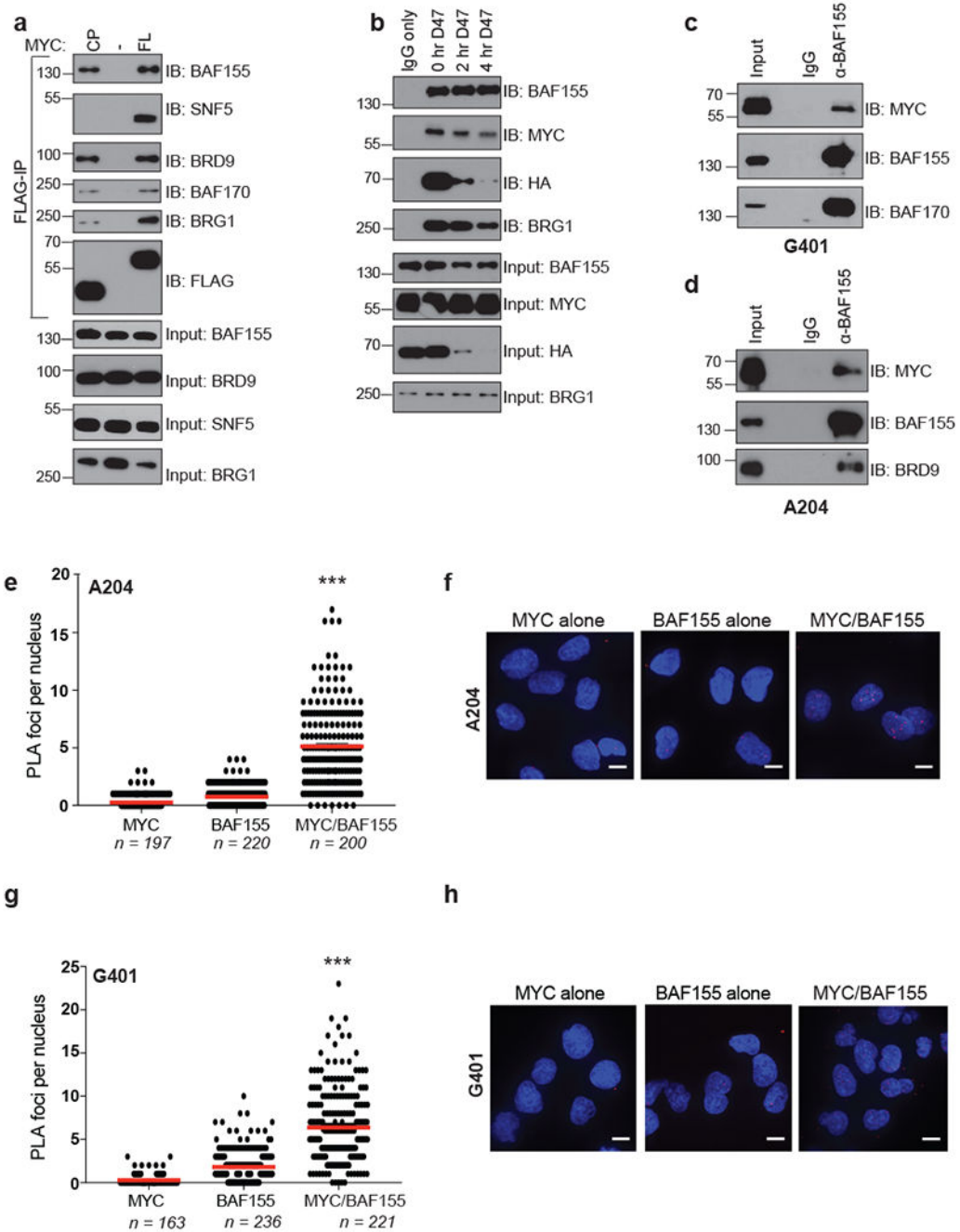


Figure 1. MYC does not require SNF5 to interact with SWI/SNF subunits.

(a) Flag-HA-epitope tagged central portion MYC (amino acids 151–319) fused to the Gal4 DNA binding domain and Flag-tagged full-length MYC were expressed into HEK293T cells, along with an empty Flag vector control. Immunoprecipitation of the central portion compared to full-length MYC reveals that SNF5 binding is specific for full-length MYC, while BRD9 co-precipitates with the central portion of MYC and full-length MYC. (b) HEK cells engineered to express a version of HA-tagged SNF5 that can be removed by the dTAG method (37) were treated with dTAG47 molecule and a BAF155 IP performed. Upon

depletion of SNF5 over time, MYC remains bound to BAF155. (c) Endogenous BAF155 was immunoprecipitated with an anti-BAF155 antibody in G401 cells. Co-immunoprecipitated material was then probed for the SWI/SNF subunit BAF170 and MYC. (d) As in (c) except the MRT cell line A204 was used and the SWI/SNF subunit BRD9 was probed as a control BAF155 interaction partner. (e) Proximity ligation assay (PLA) was performed in A204 cells and results were quantified. PLA foci detected per nucleus were counted and each data point is shown. Red bar indicates mean value per sample and n of nuclei counted appears below sample. ($n = 3$ biological replicates, error bars are standard error; *** $P < 0.001$ using unpaired t -test, two-tailed between “BAF155” and “MYC/BAF155”) (f) Representative images obtained for PLA assay in A204 cells. DAPI was used as the nuclear stain and scale bar is 10 μm . (g) Same as in (e) for G401 cells. ($n = 3$ biological replicates, error bars are standard error; *** $P < 0.001$ using unpaired t -test, two-tailed between “BAF155” and “MYC/BAF155”). (h) Representative images obtained for PLA assay as in (f) but for G401 cells.

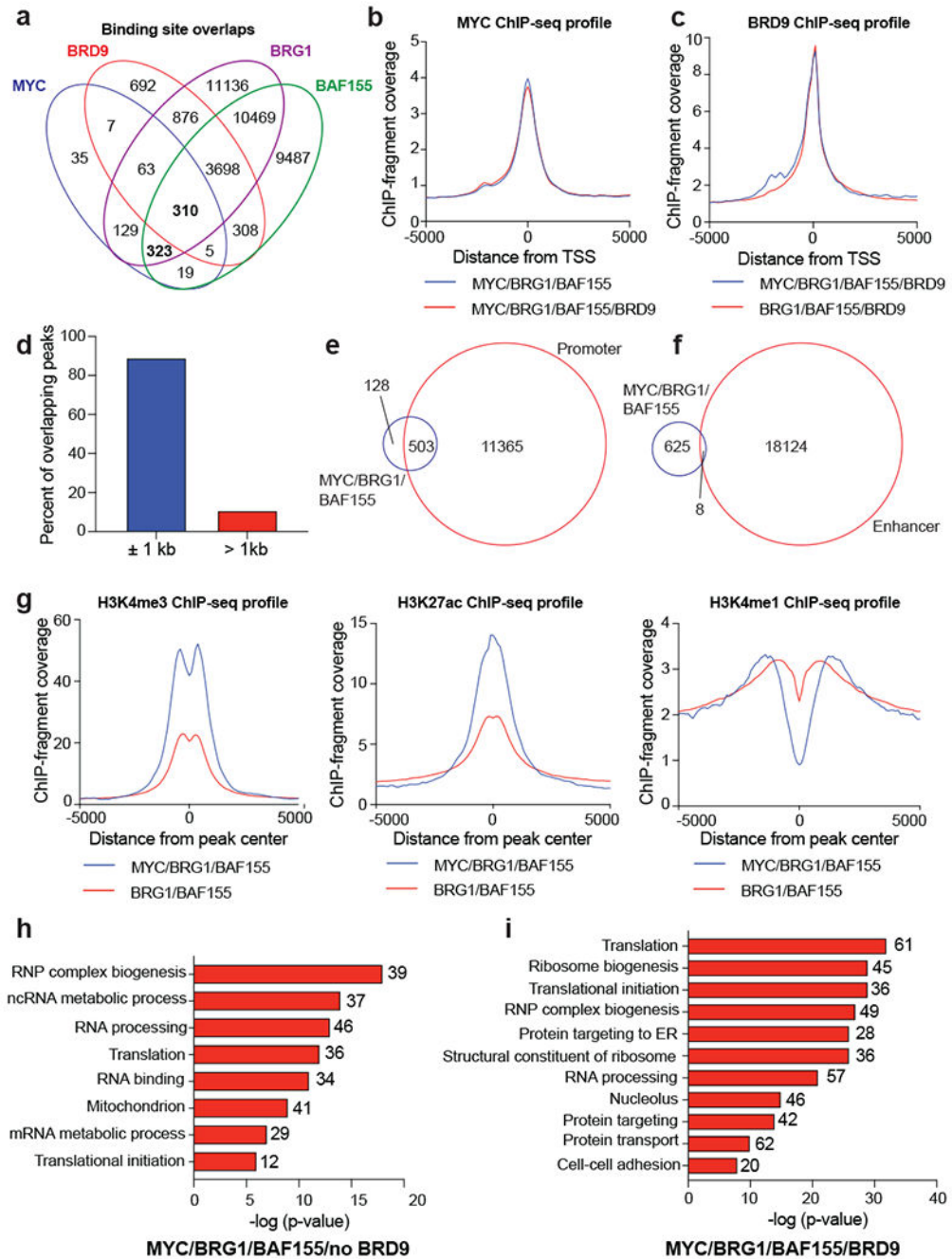


Figure 2. MYC co-localizes with SWI/SNF subunits on chromatin in malignant rhabdoid tumor cell lines.

(a) Overlap of peaks identified in published ChIP-seq data sets from three different studies in G401 cells: c-MYC (GSE109310), BAF155 and BRG1 (GSE90634), and BRD9 (GSE120235). (b) Normalized ChIP-seq fragment counts for MYC when MYC co-localizes with BRG1 and BAF155, or BRG1, BAF155, and BRD9. (c) Graph shows normalized ChIP-seq fragment counts for BRD9 when MYC is included in the overlap. (d) MYC-BRG1-BAF155 overlapped peaks (“MYC-SWI/SNF”) were annotated to determine the percent of peaks that fall within 1 kb of a transcription start site (TSS). (e) MYC-SWI/SNF

peaks were compared to peaks identified as promoters using the available data in GSE71506. Promoter regions in this data set were defined as regions that were less than 1 kb away from TSS and positive for both H3K4me3 and H3K27ac. (f) MYC-SWI/SNF peaks were compared to peaks identified as enhancers using the available data in GSE71506. Enhancer regions defined as regions that were more than 1 kb away from TSS and positive for H3K27ac without H3K4me3. (g) Normalized ChIP-seq fragment counts for H3K4me3, H3K27ac, or H3K4me1 (GSE71506) when MYC co-localizes with BRG1 and BAF155 or when BRG1 and BAF155 are without MYC. (h) Co-localized MYC-BAF155-BRG1 peaks showing no detectable BRD9 and located within 1 kb from a TSS were assigned to their nearest gene using Homer and gene ontology (GO) term enrichment analysis was performed. Numbers next to bars represents the number of genes in each group. (i) As in (h) except co-localized peaks for MYC-BAF155-BRG1-BRD9 located within 1 kb from the TSS were used for GO term enrichment analysis. RNP = ribonucleoprotein, numbers next to bars represents the number of genes in each group.

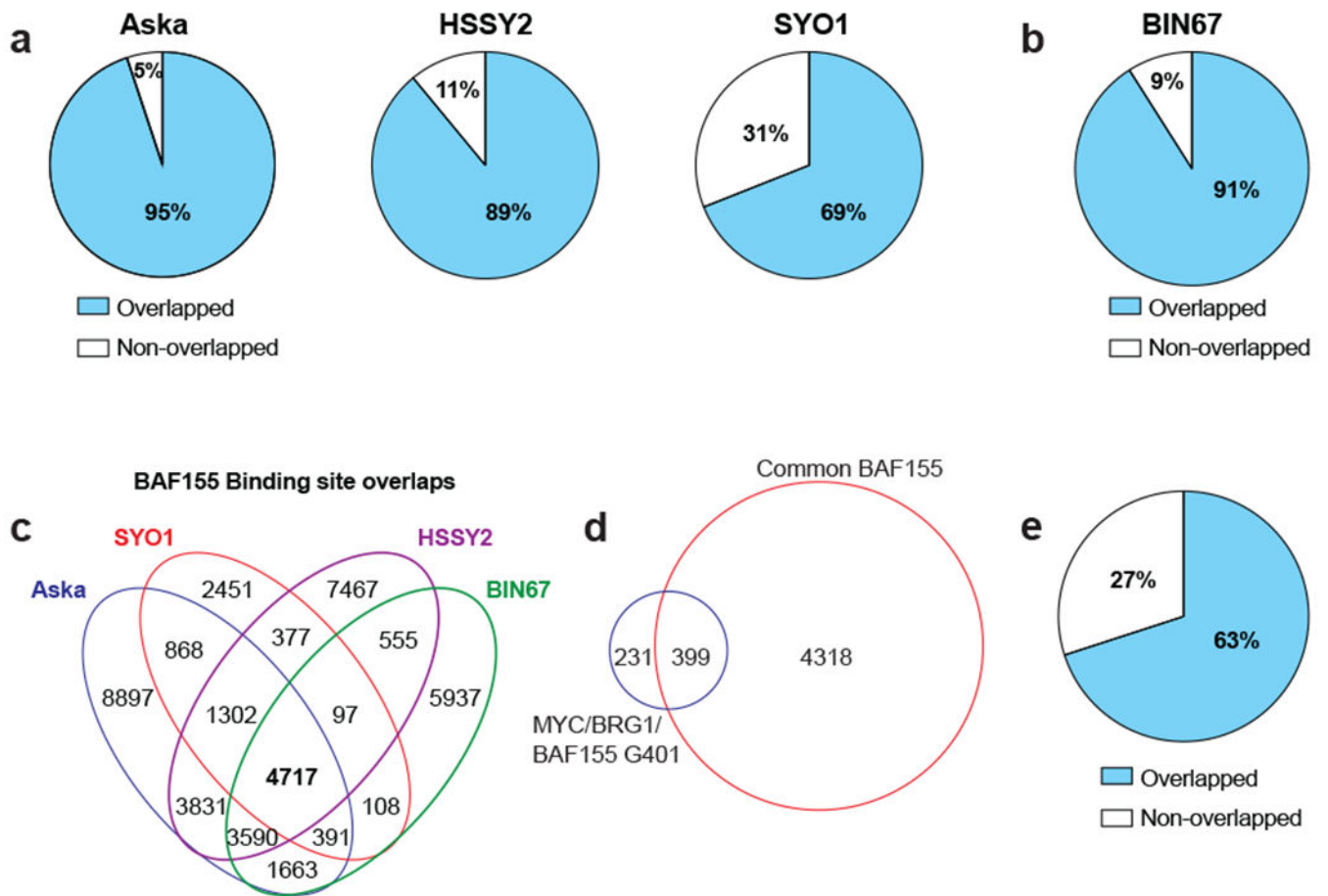


Figure 3. BAF155 is universally localized at MYC-SWI/SNF co-bound sites in other SWI/SNF altered cancers.

(a) BAF155 ChIP-seq peaks in three separate synovial sarcoma cell lines (GSE108025) were analyzed and compared to MYC-SWI/SNF peaks from Figure 2a. Pie chart shows the percent of MYC-SWI/SNF peaks that overlap with BAF155 peaks in blue. Percent of MYC-SWI/SNF peaks that are not overlapping with BAF155 peaks are shown in white. Peak numbers analyzed are reported in Supplementary Figure 1c–e. (b) BAF155 ChIP-seq peaks in the BRG1-deficient SCCOHT cell line (GSE117735) was analyzed and compared to MYC-SWI/SNF peaks from Figure 2a. Pie charts shows the percent of MYC-SWI/SNF peaks that overlap with BAF155 peaks in blue. The percent that do not overlap are shown in white and peak numbers analyzed are reported in Supplementary Figure 1f. (c) Overlap of BAF155 peaks identified in published ChIP-seq data sets from four different studies in other cancer types. Synovial sarcoma: Aska, HSSY2, and SYO1 (GSE108025). SCCOHT: BIN67 (GSE117735). (d) Overlap of 4717 common BAF155 peaks determined in (c) compared to MYC-SWI/SNF peaks in G401 cells. (e) Pie chart showing the percent of MYC-SWI/SNF peaks that overlap with common BAF155 peaks as determined in c,d. Blue denotes percent of MYC-SWI/SNF peaks that overlap with common BAF155 peaks, and white denotes the percent of MYC-SWI/SNF peaks that do not overlap with this core BAF155 set.

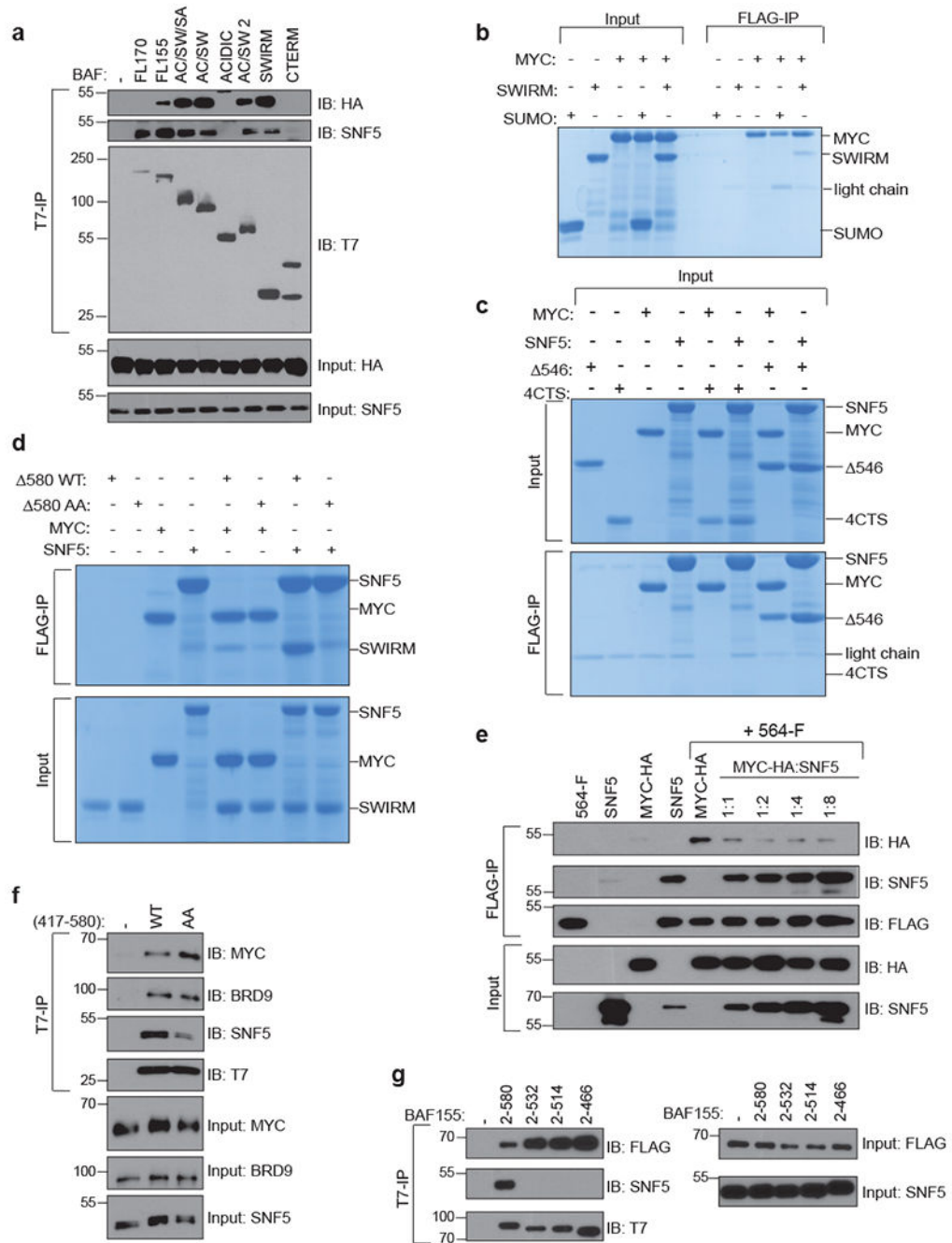


Figure 4. MYC can access SWI/SNF through interactions with the SWIRM domain of BAF155.

(a) T7-tagged BAF170, BAF155, or BAF155 domain mutants were expressed in HEK293T cells, together with the MYC central portion used in Figure 1. T7-tagged proteins were recovered by T7-IP and samples probed for HA to detect MYC or SNF5 to detect endogenous SNF5. Domains present in each BAF155 construct are denoted and listed in detail within Supplementary Figure 2. AC = acidic domain, SW = swirm domain, SA = SANT domain, CTERM = C-terminal domain. (b) Recombinant Flag-tagged MYC central portion was mixed with recombinant BAF155 SWIRM domain (amino acids 417–580 of

BAF155) or SUMO control protein and a Flag-IP performed. IP samples were eluted with 3X Flag peptide and all products, and inputs, were resolved by SDS-PAGE. Proteins visualized by Coomassie staining. Light chain of antibody used for IP shows up inconsistently in IP samples and is marked. (c) Recombinant Flag-tagged MYC central portion and Flag-tagged SNF5 were mixed with a recombinant protein containing 4 repeating sequences of the region of BAF155 corresponding to amino acids 533–546 (“4CT”). This region of BAF155 is not sufficient for binding to either MYC central portion or SNF5. Flag-IP of MYC and SNF5 with the SWIRM domain (amino acids 417–546 of BAF155: “ 546”) are shown as a control for the IP. (d) Recombinant Flag-tagged MYC central portion or Flag-tagged SNF5 were mixed with wild-type recombinant SWIRM domain (“ 580 WT) or a mutated SWIRM domain (“ 580AA”; double alanine :L534A, N536A) and Flag-IP performed as in (b). (e) Recombinant Flag-tagged SWIRM domain (amino acids 417–564 of BAF155, “546-F”), HA-tagged MYC central portion, or untagged SNF5, were mixed in the indicated molar combinations. FLAG IP was performed to recover the BAF155 SWIRM domain. Proteins were visualized by western blotting with the indicated antibodies. Beginning at a 1:1 molar ratio of SNF5:MYC, SNF5 attenuates binding of MYC central portion to the BAF155 SWIRM. (f) T7-tagged WT SWIRM domain or the “AA” mutant (amino acid mutations L534A and N536A) were expressed in HEK293T cells and T7-IP performed. (g) T7-tagged BAF155 (amino acids 1–580) or truncations targeting the SWIRM domain, were expressed in HEK293T cells along with Flag-tagged MYC and T7-IP performed. When SNF5 binding is impacted by the SWIRM truncations, Flag-tagged MYC binding increases.

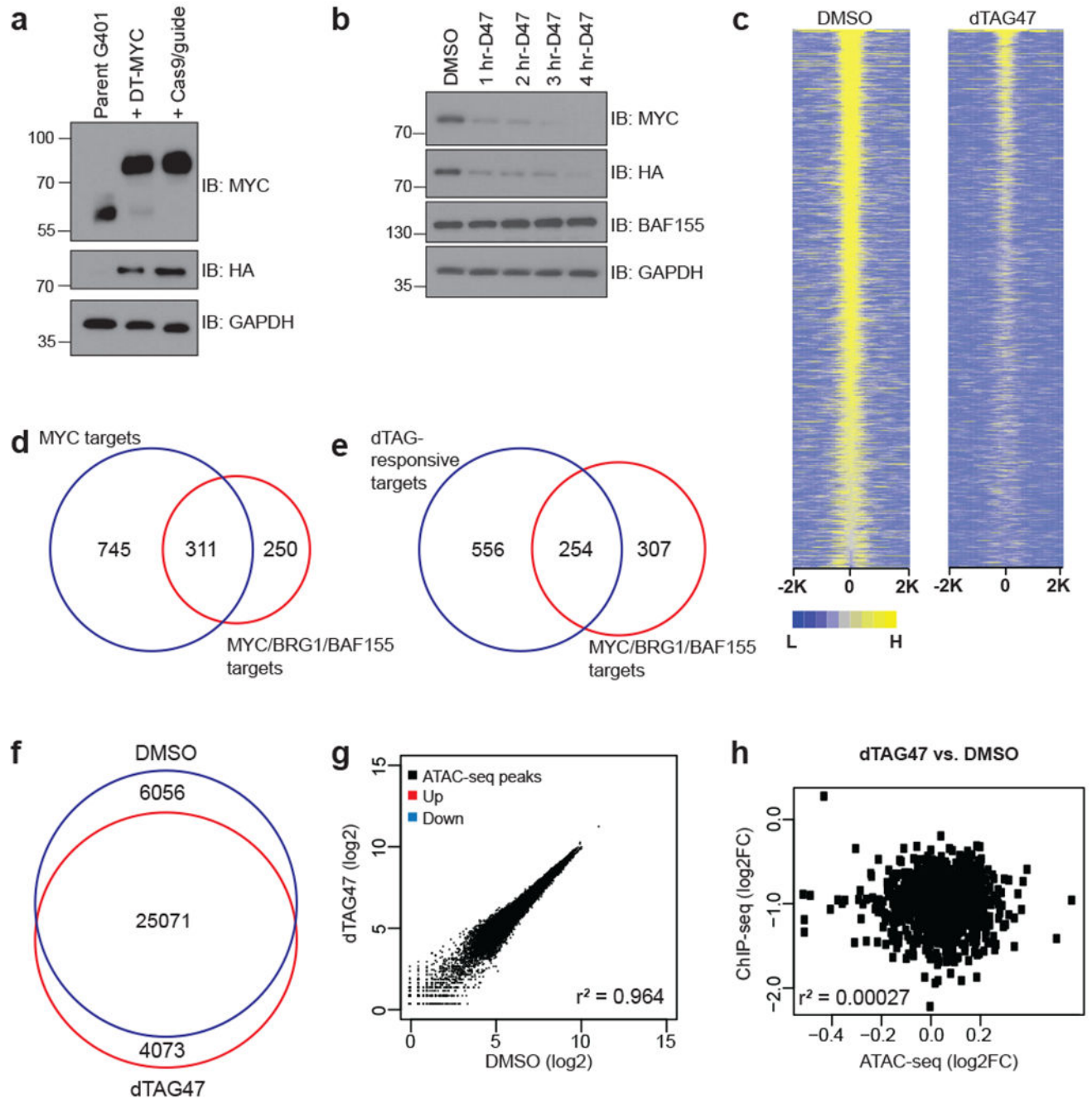


Figure 5. Engineering G401 cells to track acute changes to MYC target genes.

(a) G401 cells were transduced with a lentiviral version of c-MYC containing a N-terminal HA-FKBP12^{F36V} dTAG module: “DTMYC” (Compare *lane 1* to *lane 2*). Endogenous MYC was then removed using Cas9-CRISPR with a single guide RNA (*lane 3*). (b) Engineered DTMYC G401 cells were treated with dTAG47 for the indicated time points to induce acute degradation of MYC. “D47” indicates time of dTAG47 treatment. (c) Heat maps of HA-MYC peak intensity for DMSO or dTAG47 showing the average of normalized peak intensities in 100-bp bins within 2 kb from center of peaks. Peaks are ranked based against

DMSO. (d) Overlap between MYC/BRG1/BAF155 targets (Supplementary Table 1) with MYC targets identified in (c). Targets in both cases are defined by genes associated with peaks that fall within 1 kb of a TSS. Only unique genes included in Venn diagram. (e) Overlap between MYC/BRG1/BAF155 targets (Supplementary Table 1) with MYC targets that respond to dTAG47 addition identified in (c) and Supplementary Table 2. Targets in both cases are defined by peaks that fall within 1 kb of a TSS. Only unique genes included in Venn diagram. (f) Overlap between ATAC-seq binding sites detected in DMSO- and dTAG47-treated DTMYC G401 cells (g) Scatterplots of \log_2 -fold changes for ATAC-Seq peaks detected in dTAG47 samples compared to DMSO. (h) Scatterplot of \log_2 -fold changes for HA-MYC ChIP-Seq read counts (dTAG47/DMSO) compared to \log_2 -fold changes for ATAC-Seq read counts (dTAG47/DMSO) at all promoters. $n = 3$ independent ChIP-seq experiments. $n = 3$ independent ATAC-seq experiments.

Author Manuscript

Author Manuscript

Author Manuscript

Author Manuscript

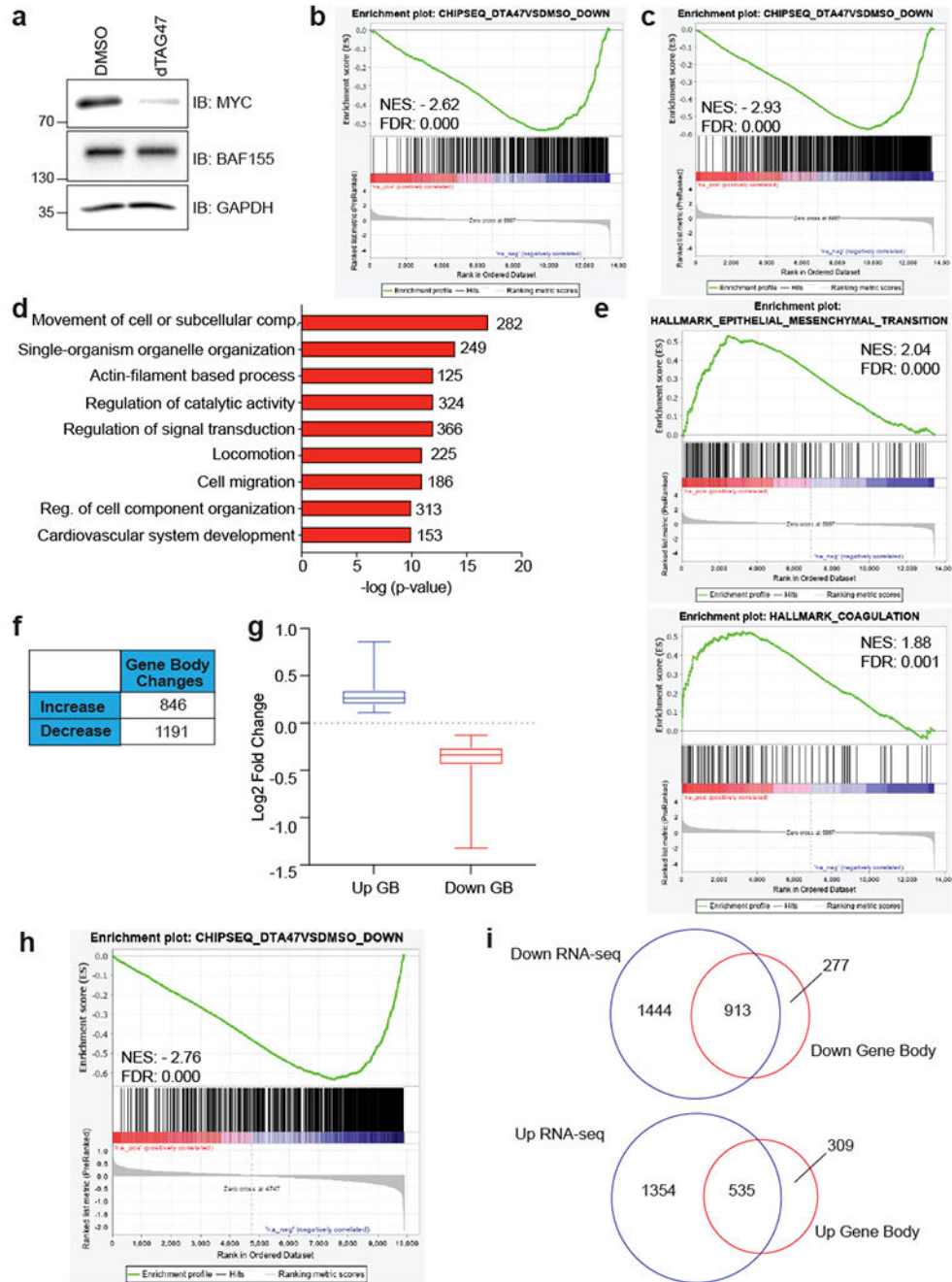


Figure 6. MYC loss results in widespread gene expression changes.

(a) Engineered G401 cells were treated with dTAG47 for 24 hours to selectively deplete MYC. (b) Gene set enrichment analysis of MYC targets significantly changed by dTAG47 addition as determined by ChIP-seq (FDR < 0.05, 2-fold change) compared to a ranked list of gene expression changes from RNA-seq. (c) Gene set enrichment analysis of MYC targets significantly changed by dTAG47 addition as determined by ChIP-seq (FDR < 0.05) compared to a ranked list of gene expression changes from RNA-seq. (d) GO-term enrichment analysis of genes up-regulated by dTAG47 treatment. Numbers next to bars

represents the number of genes in each group. (e) Gene set enrichment analysis of all gene expression changes against the MSigDB gene set hallmark data sets “epithelial-mesenchymal transition” and “coagulation” (f) The number of genes showing a significant change in gene body associated RNA polymerase as determined by PRO-Seq. (g) Log₂-fold changes for genes with an increase (“Up GB”) or decrease (“Down GB”) in gene body associated RNA polymerase. Box-and-whisker plot shows the 25th to 75th percentile with the median marked by the middle line and whiskers extending from maximum to minimum point. (h) Gene set enrichment analysis of MYC targets significantly changed by dTAG47 addition as determined by ChIP-seq (FDR < 0.05) compared to a ranked list of genes with decrease RNA polymerase as determined by PRO-Seq. (i) Overlap between down-regulated transcripts (top) or up-regulated transcripts (bottom) with gene body changes. Only unique genes included in Venn diagram. $n = 3$ independent RNA-seq experiments, $n = 2$ independent PRO-Seq experiments.

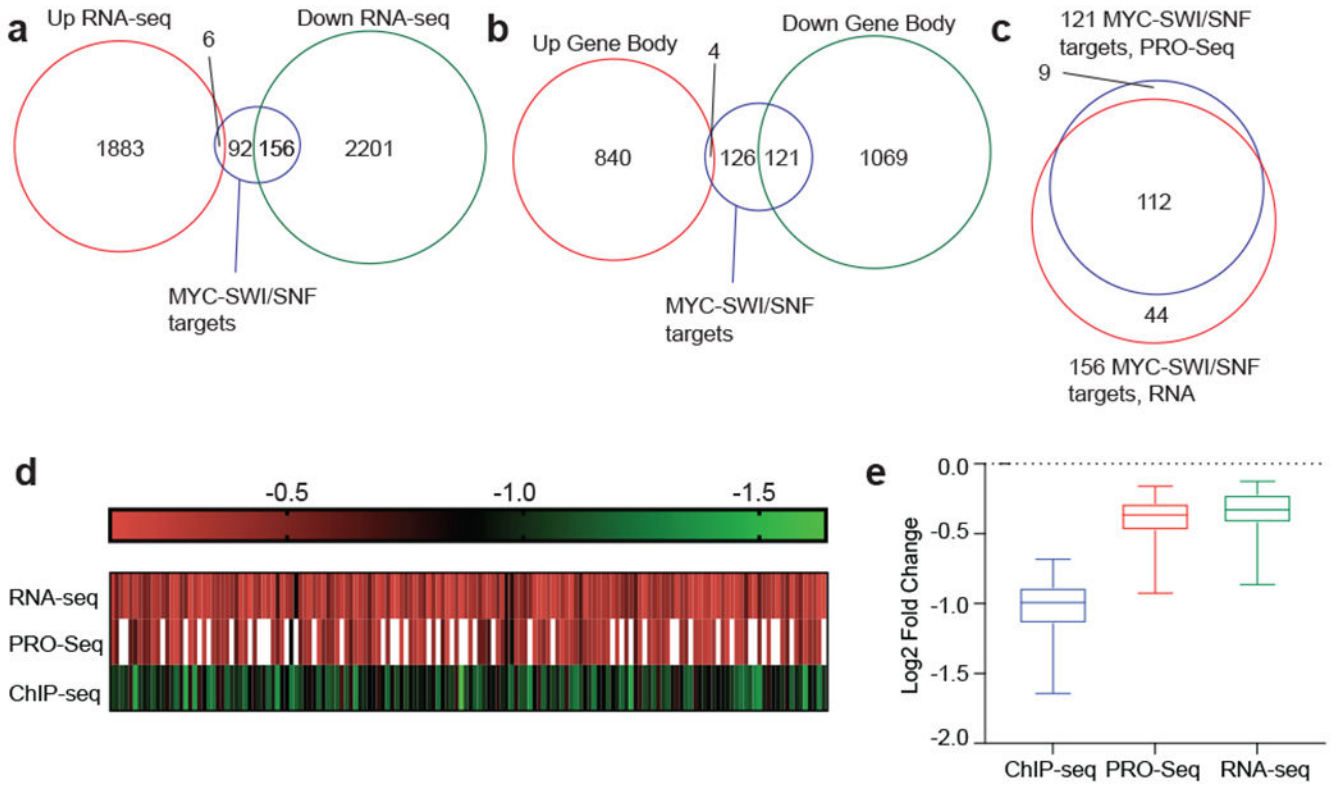


Figure 7. Impact of MYC loss on MYC-SWI/SNF target gene expression.

(a) Overlap between RNA-seq gene expression changes and MYC-SWI/SNF targets regulated by dTAG47 (Fig. 5e). Only unique genes included in Venn diagram. (b) Overlap between PRO-seq gene body changes and MYC-SWI/SNF targets regulated by dTAG47. Only unique genes included in Venn diagram. (c) Overlap between MYC-SWI/SNF targets down-regulated in (a) with those down-regulated in (b). (d) Heatmap of 156 MYC-SWI/SNF targets from (a) showing \log_2 -fold changes for each gene as determined by ChIP-seq, PRO-Seq, and RNA-seq. (e) \log_2 -fold changes for genes from (d). Box-and-whisker plot shows the 25th to 75th percentile with the median marked by the middle line and whiskers extending from maximum to minimum point.